

## BIOCHEMISTRY

# Rhodoxanthin synthase from honeysuckle; a membrane diiron enzyme catalyzes the multistep conversion of $\beta$ -carotene to rhodoxanthin

John Royer<sup>1\*</sup>, John Shanklin<sup>2</sup>, Nathalie Balch-Kenney<sup>1</sup>, Maria Mayorga<sup>1</sup>, Peter Houston<sup>1</sup>, René M. de Jong<sup>3</sup>, Jenna McMahon<sup>1</sup>, Lisa Laprade<sup>1</sup>, Paul Blomquist<sup>1</sup>, Timothy Berry<sup>1</sup>, Yuanheng Cai<sup>2</sup>, Katherine LoBuglio<sup>4</sup>, Joshua Trueheart<sup>1†</sup>, Bastien Chevreux<sup>1‡</sup>

Rhodoxanthin is a vibrant red carotenoid found across the plant kingdom and in certain birds and fish. It is a member of the atypical retro class of carotenoids, which contain an additional double bond and a concerted shift of the conjugated double bonds relative to the more widely occurring carotenoid pigments, and whose biosynthetic origins have long remained elusive. Here, we identify LHRs (*Lonicera* hydroxylase rhodoxanthin synthase), a variant  $\beta$ -carotene hydroxylase (BCH)-type integral membrane diiron enzyme that mediates the conversion of  $\beta$ -carotene into rhodoxanthin. We identify residues that are critical to rhodoxanthin formation by LHRs. Substitution of only three residues converts a typical BCH into a multifunctional enzyme that mediates a multistep pathway from  $\beta$ -carotene to rhodoxanthin via a series of distinct oxidation steps in which the product of each step becomes the substrate for the next catalytic cycle. We propose a biosynthetic pathway from  $\beta$ -carotene to rhodoxanthin.

## INTRODUCTION

Rhodoxanthin (4',5'-didehydro-4,5'-retro- $\beta$ ,  $\beta$ -carotene-3,3'-dione) is a brilliant red pigment that is widely but sporadically represented in nature. It is a member of an atypical family of carotenoids that contain a register shift in the alternating pattern of double and single bonds relative to that of the more widely occurring carotenoids and are therefore referred to as retro-carotenoids (compare Fig. 1, A and B) (1). In retro-carotenoids, the rings are more planar relative to the polyene backbone, resulting in increased conjugation that changes the vibrational modes of the molecule, resulting in altered vibrational spectra relative to other carotenoids (2). In rhodoxanthin, the carotene ring C3 and C3' carbons are ketolated, the double bonds of which contribute additional conjugation, while in eschscholtzanthin, a retro-carotenoid found in California poppy, the C3 and C3' carbons are, instead, hydroxylated (Fig. 1A) (3).

Rhodoxanthin has been observed in the sun-stressed leaves of a number of conifers (4) as well as in similarly stressed leaves of angiosperms in the genus *Aloe* (5). The feathers of a small number of bird species accumulate rhodoxanthin, in some cases, due to conversion of consumed zeaxanthin or lutein precursors (2) and, in other cases, due to the dietary consumption of rhodoxanthin-containing plants (6, 7). Rhodoxanthin accumulates notably and at high levels in the arils of yew (*Taxus* sp.) (8) and in the berries of certain species of honeysuckle (*Lonicera* sp.) (9).

The pathways and enzymes leading to the major plant carotenoids are well defined and are the subject of several excellent reviews, e.g., (10–12). Lycopene, the first colored compound in the carotenoid pathway, is modified by distinct cyclases to produce either

$\beta$ -carotene or  $\alpha$ -carotene.  $\beta$ -Carotene is converted to zeaxanthin by  $\beta$ -carotene hydroxylase (BCH), an integral membrane diiron monooxygenase in the fatty acid hydroxylase superfamily of enzymes (Fig. 1B) (13). BCH variants are found within chloroplasts of photosynthetic tissue and within chromoplasts of fruits and flowers (14).

While the biosynthetic routes to the major plant carotenoids are well established, the enzymes and pathway(s) to retro-carotenoids have remained elusive. In the absence of enzymatic or genetic investigations, proposed routes have been based on chemical composition analyses of carotenoid-containing material (8, 15). Here, we have identified and characterized LHRs (*Lonicera* hydroxylase rhodoxanthin synthase), a previously unreported variant of the BCH family of enzymes that confers rhodoxanthin biosynthetic capability when expressed in a rhodoxanthin-lacking plant expression system and a  $\beta$ -carotene-accumulating bacterial expression system. LHRs both hydroxylates  $\beta$ -carotene and catalyzes the unique ketolations, desaturation, and double bond rearrangement required for rhodoxanthin biosynthesis. In addition, we have identified key specificity-determining residues that are responsible for conferring the rhodoxanthin-biosynthesizing capability to the honeysuckle enzyme. Confirmation of the influence of these residues was obtained by the demonstration that their introduction into equivalent positions of a tomato BCH conferred rhodoxanthin-synthesizing activity. Last, we have identified previously unreported pathway intermediates, allowing us to propose a pathway from  $\beta$ -carotene to rhodoxanthin. To our knowledge, this is the first identification of a gene coding for a multifunctional enzyme responsible for the synthesis of a retro-carotenoid.

## RESULTS

### Confirmation of rhodoxanthin in red *Lonicera* berries

On the basis of previous studies (9), *Lonicera* berries were selected to study rhodoxanthin biosynthesis. Extracts from red and orange berries from two *Lonicera* plants (Bolton Red and Bolton Orange) growing at the same location were separated by high-performance liquid chromatography (HPLC) and analyzed by photodiode array (PDA) spectroscopy with the use of synthetic rhodoxanthin as standard.

<sup>1</sup>DSM Nutritional Products, 60 Westview St, Lexington, MA 02421, USA. <sup>2</sup>Department of Biology, Brookhaven National Laboratory, 50 Bell Ave, Upton, NY 11973, USA.

<sup>3</sup>DSM Biotechnology Center, Alexander Fleminglaan 1, 2613 AX Delft, Netherlands.

<sup>4</sup>Department of Organismic and Evolutionary Biology, Farlow Herbarium of Cryptogamic Botany, Harvard University, 22 Divinity Avenue, Cambridge, MA 02138, USA.

\*Corresponding author. Email: john.royer@dsm.com

†Present address: Ginkgo Bioworks, 27 Drydock Avenue, Boston, MA 02210, USA.

‡Present address: Bayer AG Information Technology Digital Transformation & IT Strategy Building S160, 0/050, 13342 Berlin, Germany.

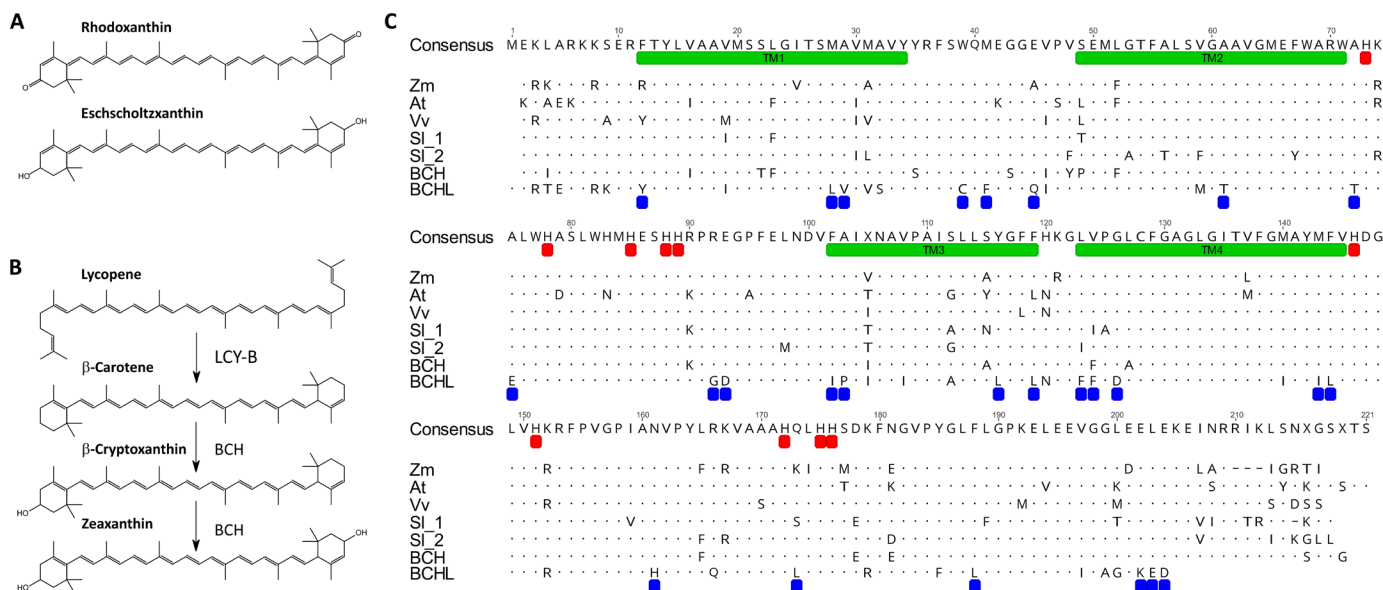


**Fig. 1. Retro-carotenoid structures, carotenoid structures, and their established relationships illustrating the role of BCH and a sequence alignment of BCH enzymes from *Lonicera* with those of other plants.** (A) Structure of the retro-carotenoids rhodoxanthin and eschscholtzanthin. (B) Pathway from lycopene to  $\beta$ -carotene,  $\beta$ -cryptoxanthin, and zeaxanthin in plants. LCY-B, lycopene  $\beta$ -cyclase, EC (Enzyme Commission) 5.5.1.19; BCH,  $\beta$ -carotene hydroxylase, EC 1.14.13.129. (C) Alignment of *Lonicera* BCHL and BCH with other plant BCHs. Aligned sequences represent mature proteins after cleavage of the presumed plastid-targeting sequence. Residues with dots are identical to the consensus amino acid. Green regions below the consensus sequence indicate predicted transmembrane domains, and red boxes indicate conserved histidine residues. Blue boxes below LHRS indicate residues that differed between BCHs and LHRS. Accession numbers and regions included in alignment are as follows: Zm (*Z. mays* ZMCRTRB3), AFD18929 (100-312); At (*A. thaliana* BCH2), NP\_200070 (84-303); Vv (*V. vinifera* BCH1), NP\_001268126 (84-299); SL\_1 (*S. lycopersicum* CRTR-B1), NP\_001234348 (94-309); SL\_2 (*S. lycopersicum* CRTR-B2), CAB55626 (98-314); *Lonicera* BCH, MK982903 (93-310); *Lonicera* BCHL, MK982903 (82-285). BCHL was later renamed LHRS.

As shown in fig. S1A, the (heated) rhodoxanthin standard eluted as three distinct isomers (6Z, 6'Z; 6Z, 6'E; and 6E, 6'E) with the expected corresponding spectra (2). The profile corresponding to the Bolton Red berry extracts (fig. S1B), along with profiles from extracts of red berries obtained from a different site (Lex Red), contained major carotenoid species that coeluted with those of the authentic rhodoxanthin standard. Bolton Orange berries lacked these species and contained instead major species with elution times characteristic of  $\beta$ -cryptoxanthin and zeaxanthin (fig. S1C).

### Identification of a highly expressed BCH homolog from red berries

A combined transcriptomic and proteomic approach was used to identify candidate factor(s) that related to rhodoxanthin synthesis. mRNAs corresponding to several genes involved in carotenoid biosynthesis were detected in both ripe red berries and green leaves from a single *Lonicera* plant (Lex Red). However, we identified a BCH-like gene (*BCHL*) that was highly expressed in red berries but barely detected in leaf tissue. In contrast, a second BCH gene (*BCH*) was expressed in both tissues (table S1). We next compared the proteomes corresponding to extracts of the ripe red and ripe orange berries characterized in fig. S1. As shown in Table 1, the levels of many carotenoid biosynthetic enzymes were similar in both red and orange berries, whereas *BCHL* expression was much stronger in red relative to orange berries.

### Sequence analysis of *BCHL*

As shown in Fig. 1C, *Lonicera* *BCHL* is homologous to previously described plant BCH enzymes. It contains the conserved histidine boxes and predicted transmembrane domains characteristic of the

fatty acid desaturase/hydroxylase superfamily (16). However, *BCHL* contained nonconserved residues at several locations that are highly conserved among known BCHs. These results raised the possibility that the catalytic activity of *BCHL* might be different from that of the well-characterized BCHs. In contrast, the sequence of *Lonicera* *BCH* closely matches consensus amino acid identities at these positions, consistent with it being a more typical BCH. Phylogenetic analysis confirmed that *BCH* clusters with typical plant BCH genes, while *BCHL* is an outlier with earlier divergence from a common ancestor (fig. S2).

### *BCHL* activity in *Nicotiana benthamiana* transient expression system

To test the effect of *BCHL* in a non-rhodoxanthin-producing plant, we transfected *N. benthamiana* with full-length *BCHL* complementary DNA (cDNA). As shown in fig. S3, extracts of leaves transfected with *BCHL* contained three chemical species that eluted at times characteristic of the corresponding authentic rhodoxanthin isomers with the same absorption profiles, while the control leaves lacked them. These results are consistent with *BCHL* facilitating rhodoxanthin biosynthesis in a plant background.

### Activity of *BCHL* in *Escherichia coli*

It was not feasible to identify the substrate for *BCHL* in *N. benthamiana* because its leaves contain a diverse ensemble of carotenoids. To confirm the ability of *BCHL* to synthesize rhodoxanthin and to elucidate its biosynthetic pathway, we developed a three-plasmid *E. coli* expression system (see Materials and Methods). A  $\beta$ -carotene-accumulating *E. coli* strain (MB8167) harboring *Pantoea agglomerans* Eho10 genes for lycopene synthesis (17) and a truncated version of

**Table 1. Proteomic analysis of carotenoid biosynthesis enzymes in chromoplast-enriched fractions of red (Bolton Red) and orange (Bolton Orange) *Lonicera* berries.** Chromoplast-enriched fractions were prepared from berry extracts using Nycodenz gradients as described in Materials and Methods. Numbers represent protein intensities (sparse) as described in Materials and Methods.  $\beta$ -Tubulin is included as control. BCHL was subsequently renamed LHRS.

	Red	Orange	Red/orange
Geranylgeranyl pyrophosphate synthase	5,504	7,230	0.8
Prolycopene isomerase	33,303	30,639	1.1
Phytoene dehydrogenase	131,947	221,823	0.6
$\zeta$ -Carotene desaturase	97,890	164,652	0.6
Lycopene cyclase	335,719	485,908	0.7
$\beta$ -Carotene hydroxylase-like (BCHL)	48,365	326	148.2
Carotenoid cleavage dioxygenase	590,400	447,943	1.3
$\beta$ -Tubulin	161,357	148,729	1.1

a *Lonicera*  $\beta$ -carotene cyclase *LCY-B* was constructed. Strain MB8167 was transformed with a separate plasmid containing truncated *BCHL* lacking the presumed plastid-targeting signal to generate strain MB8173. As shown in Figs. 2 and 3A, after 36 hours of culture, MB8173 accumulated a mixture of carotenes,  $\beta$ -cryptoxanthin, zeaxanthin, and rhodoxanthin isomers. The HPLC trace contained the three rhodoxanthin isomer peaks corresponding to those derived from the authentic rhodoxanthin standard (fig. S1). On the basis of its ability to confer rhodoxanthin biosynthesis in plant and *E. coli* expression systems, we have renamed *BCHL* *Lonicera* hydroxylase rhodoxanthin synthase (*LHRS*).

### Identification of specificity-determining residues for rhodoxanthin biosynthesis in LHRS

We hypothesized that some of the differences in amino acid identities found in LHRS relative to conserved locations within BCH enzymes (Fig. 1C) are responsible for its rhodoxanthin-synthesizing activity. To test this, a preliminary screen was performed in which the residues at 23 LHRS locations were individually substituted with the equivalent conserved BCH residue. As shown in table S2, expression of 10 of the 23 individual LHRS mutants led to reduced levels of rhodoxanthin relative to  $\beta$ -cryptoxanthin and zeaxanthin, identifying those residues as contributing to rhodoxanthin biosynthesis.

### Conversion of tomato BCH to a rhodoxanthin-synthesizing enzyme

To test the importance of the above 10 LHRS residues with respect to rhodoxanthin synthesis, we substituted all 10 LHRS residues into the equivalent positions in a typical zeaxanthin-generating BCH enzyme, the chromoplastic BCH CRTR-B2 from *Solanum lycopersicum* (14), to create CRTR-B2\_10. While expression of native CRTR-B2 resulted in the accumulation of  $\beta$ -cryptoxanthin and zeaxanthin, expression of CRTR-B2\_10 resulted in accumulation of rhodoxanthin in addition to the hydroxylated products (Fig. 3B).

To evaluate the contributions of each of the 10 residues, we created clones in which each was individually reverted to that found in the consensus BCH sequence (fig. S4). Expression of these constructs in *E. coli* showed that Thr<sup>72</sup>, Ile<sup>102</sup>, and Pro<sup>103</sup> were most influential for rhodoxanthin formation. We next introduced these three residues individually, or in combinations thereof, into the

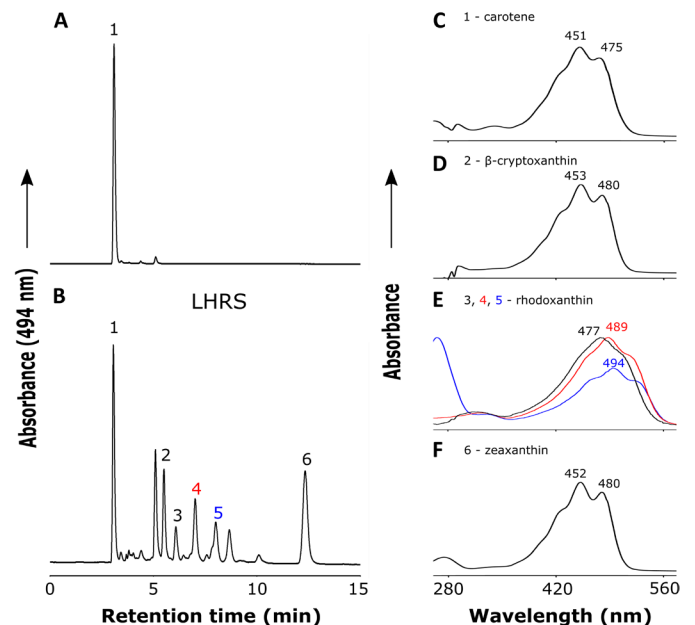


**Fig. 2. HPLC separation and PDA spectra of carotenoids in extracts of *E. coli* expressing bacterial lycopene biosynthetic genes, *Lonicera* *LCYB*, and *Lonicera* *BCHL*.** (A and C) *E. coli* expressing CrE (geranylgeranyl diphosphate synthase), CrI (phytoene dehydrogenase), CrB (phytoene synthase), and Idi (isopentenyl-diphosphate  $\delta$ -isomerase) from *P. agglomerans* and *LCYB* (lycopene  $\beta$ -cyclase) from *Lonicera* sp. (B and D to F) *E. coli* expressing CrE, CrB, CrI, and Idi from *P. agglomerans*, *LCYB* from *Lonicera*, and LHRS of *Lonicera*. Peak 1, carotenes; 2,  $\beta$ -cryptoxanthin; 3, rhodoxanthin 6Z, 6'Z isomer; 4, rhodoxanthin 6Z, 6'E isomer; 5, rhodoxanthin 6E, 6'E isomer; 6, zeaxanthin. Absorbance at 494 nm is shown on the y axis, and time in minutes is shown on the x axis. Strains were grown for 36 hours on inducing medium, extracted, and analyzed by normal-phase HPLC as described in Materials and Methods. *BCHL* was later renamed *LHRS*.

wild-type BCH, CRTR-B2 (fig. S5). A single amino acid substitution of Phe at Ile<sup>102</sup> in wild-type CRTR-B2 resulted in the accumulation of detectable rhodoxanthin. The combination of either A72T or A103P, or most effectively both, with F102I resulted in rhodoxanthin accumulation at similar levels to that observed for CRTR-B2\_10, confirming that these three positions play a major role in rhodoxanthin formation (Fig. 3B and fig. S5).

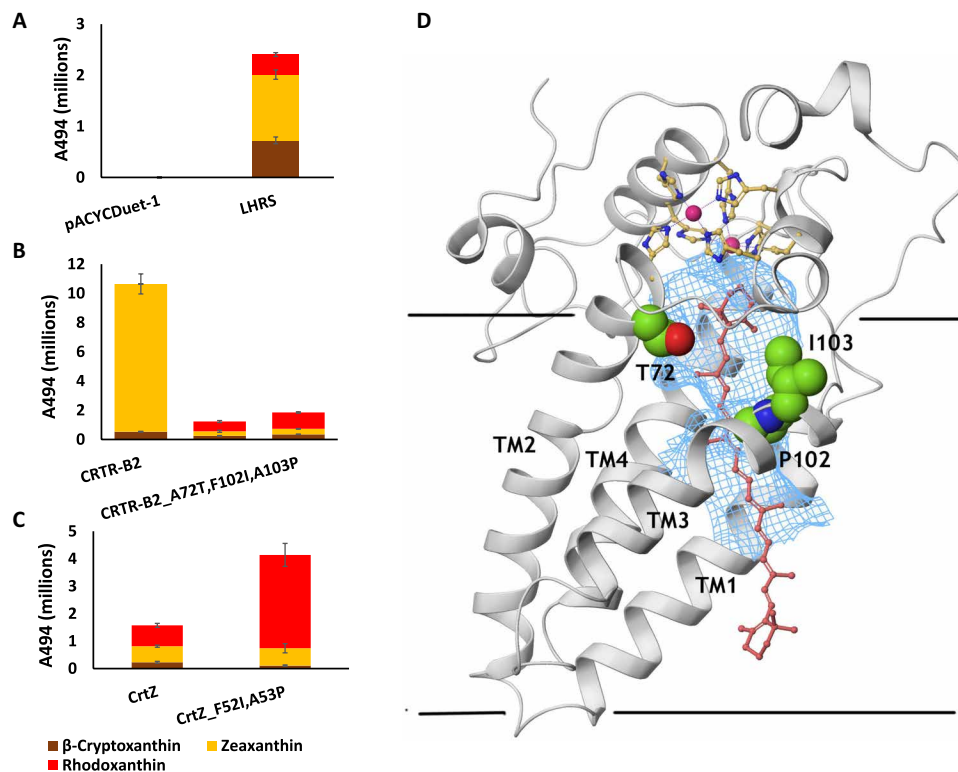


**Fig. 3. The effects of expression of BCH genes, and mutants thereof, on xanthophyll accumulation in *E. coli*, along with a cartoon representation of LHRS to illustrate the relative orientation of key residues that influence rhodoxanthin formation.** Xanthophyll accumulation in *E. coli* expressing (A) empty vector control (pACYCDuet-1) and honeysuckle enzyme LHRS; (B) *S. lycopersicum* chromoplast BCH gene CRTR-B2, CRTR-B2\_10 (CRTR-B2 M28L, A29V, 61T, A72T, F102I, A103P, G126D, M143I, F144L, and Q173L) and CRTR-B2 A72T, F102I, A103P; and (C) BCH of *P. agglomerans* (CrtZ) and CrtZ F52I, F53P. Strains were transformed into β-carotene-producing strain MB8167 expressing *P. agglomerans* genes for lycopene production [*crtE* (geranylgeranyl diphosphate synthase), *crtI* (phytoene dehydrogenase), *crtB* (phytoene synthase), and *idi* (isopentenyl-diphosphate δ-isomerase)] along with *LCY-B* (lycopene β-cyclase) from *Lonicera*. Data points are mean and SE of three biological replicates. Strains were grown on inducing medium, extracted, and analyzed by normal-phase HPLC as described in Materials and Methods. (D) A cartoon representation of the LHRS model structure embedded in the membrane showing the location of the three substitution sites, which control rhodoxanthin formation in LHRS, in green CPK representation. The strictly conserved catalytic His-metal clusters are shown in ball-and-stick representation. A cavity leading toward the catalytic His-metal cluster is shown as a blue mesh. The approximate boundaries of the membrane are shown as black bars.

### Rhodoxanthin synthesis by bacterial CrtZ

As an independent test of the three specificity-determining residues, we investigated the more distantly related bacterial BCH, CrtZ, from *P. agglomerans* (*Erwinia herbicola* Eho10) (18), which shares only 36% identity to LHRS, lacks one of the membrane-spanning domains common to LHRS and plant BCHs, and naturally contains Thr at residue 22, the location equivalent to T72 of LHRS. Under our experimental conditions, expression of the native enzyme in the β-carotene-producing *E. coli* strain MB8167 resulted in the accumulation of rhodoxanthin, in addition to β-cryptoxanthin and zeaxanthin (Fig. 3C). Substitution of F52I and A53P created the most specific rhodoxanthin-forming activity identified to date. This experiment provides independent support for the involvement of the three residues in rhodoxanthin formation.

### Structural model of LHRS

We present a structural model (Fig. 3D) of LHRS based on the crystal structure of the yeast sphingolipid hydroxylase Scs7P (19). In this model, the previously identified group of eight conserved histidine residues (see Fig. 1C) superimpose with equivalent sites in the crystal structure of the fatty acid α-hydroxylase that coordinate the

conserved dimetal center. The model has a long deep channel, extending from the outside of the enzyme to the dimetal active site, which is large enough to accommodate most of a β-carotene substrate molecule. Key residues that contribute to rhodoxanthin formation, 102 and 103, are located at the end of one helix, while the third key residue, 72, is positioned at the end of another helix adjacent to His<sup>73</sup>, which is a metal-coordinating ligand residue. The proximity of these sites to the presumed substrate-binding cavity and dimetal center is consistent with their experimentally defined roles in rhodoxanthin formation described above.

### Identification of intermediates and proposed pathway of β-carotene to rhodoxanthin

A time course of carotenoid formation in *E. coli* expressing LHRS showed sequential accumulation of carotenes, β-cryptoxanthin, zeaxanthin, and rhodoxanthin (Fig. 4A). To investigate the biochemical pathway from β-carotene to rhodoxanthin in more detail, we analyzed carotenoid formation in *E. coli* cultures expressing the more active CrtZ\_F52I, A53P with the use of mass spectrometry (MS). The CrtZ\_F52I, A53P time course showed sequential accumulation of β-cryptoxanthin, zeaxanthin, three unknowns (Cmpds I, II, and III), and finally rhodoxanthin (Fig. 4B). While difficult to

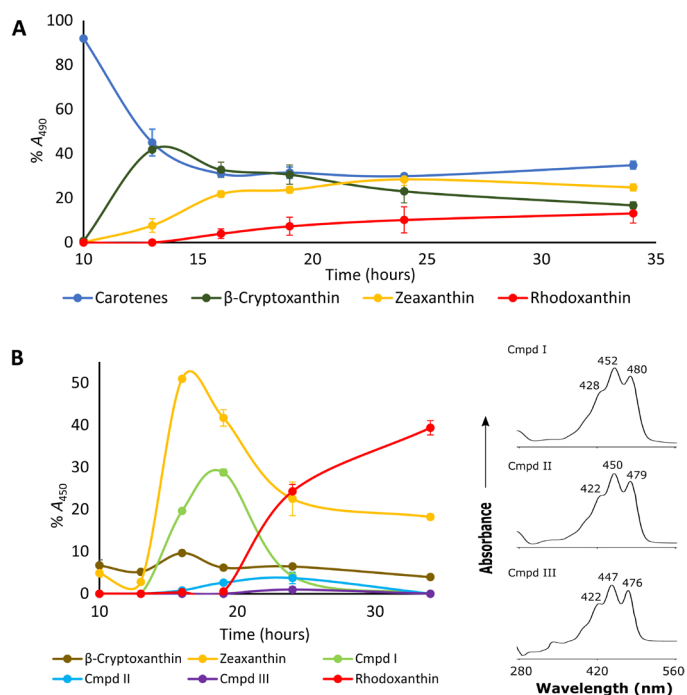


**Fig. 4. Formation of carotenoid intermediates and rhodoxanthin in *E. coli* cultures expressing LHRS and *P. agglomerans* CrtZ\_F52I, A53P.** (A) Time course of carotenoid accumulation in *E. coli* cultures expressing LHRS and CrtZ\_F52I,A53P. (B) Time course and PDA spectra of carotenoids accumulating during expression of CrtZ\_F52I,A53P. Cmpd I, identified as  $\beta$ ,  $\beta$ -carotene-3-ol,3'-keto; Cmpd II, identified as  $\beta$ ,  $\beta$ -carotene-3,3'-dione; and Cmpd III; identified as  $\beta$ ,  $\epsilon$ -carotene-3,3'-dione. *E. coli* also expresses *crtE* (geranylgeranyl diphosphate synthase), *crtI* (phytoene dehydrogenase), *crtB* (phytoene synthase), and *idi* (isopentenyl-diphosphate  $\delta$ -isomerase) from *P. agglomerans* along with truncated *LCY-B* (lycopene  $\beta$ -cyclase) from *Lonicera* (see tables S3 and S4 and fig. S6). Strain was grown on inducing medium and analyzed by normal-phase HPLC as described in Materials and Methods. Data points are the average  $\pm$  SD of three replicates.

visualize in PDA chromatograms, Cmpds I, II, and III were also detected by MS in *E. coli* cultures expressing LHRS and CrtR-B2\_10 and at low levels in ripening red *Lonicera* berries (see table S4).

We have used a combination of liquid chromatography–MS, spectral properties, and order of appearance (Fig. 4B, fig. S6, and table S3) to tentatively identify Cmpds I, II, and III and propose a pathway from  $\beta$ -carotene to rhodoxanthin (Fig. 5). The mass (566) and predicted formula ( $C_{40}H_{54}O_2$ ) for Cmpd I is consistent with the loss of two hydrogens from zeaxanthin (mass 568), which could result from either the conversion of a hydroxyl group to a keto group on one of the rings or a desaturation event within the  $\beta$ -carotene backbone. The spectrum of Cmpd I matches that of zeaxanthin (see Fig. 2), consistent with retention of the  $\beta$ -carotene backbone, implying that Cmpd I is likely the result of a further oxidation of one of the ring hydroxyls to a keto group rather than a desaturation event on the carotene backbone. On the basis of these observations, we have tentatively identified Cmpd I as  $\beta$ , $\beta$ -carotene-3-ol,3'-one (see Fig. 5). Similarly, the mass (564), predicted formula ( $C_{40}H_{52}O_2$ ), and zeaxanthin-like PDA spectrum for Cmpd II are consistent with a second oxidation of a hydroxyl to a keto group on the remaining hydroxyl-containing ring of Cmpd I. Cmpd II is tentatively identified as  $\beta$ , $\beta$ -carotene-3,3'-dione (see Fig. 5). Cmpd III, which is present in low amounts at the 24-hour time point, is identical in mass to Cmpd II, but its PDA spectrum is distinguished by a hypochromic

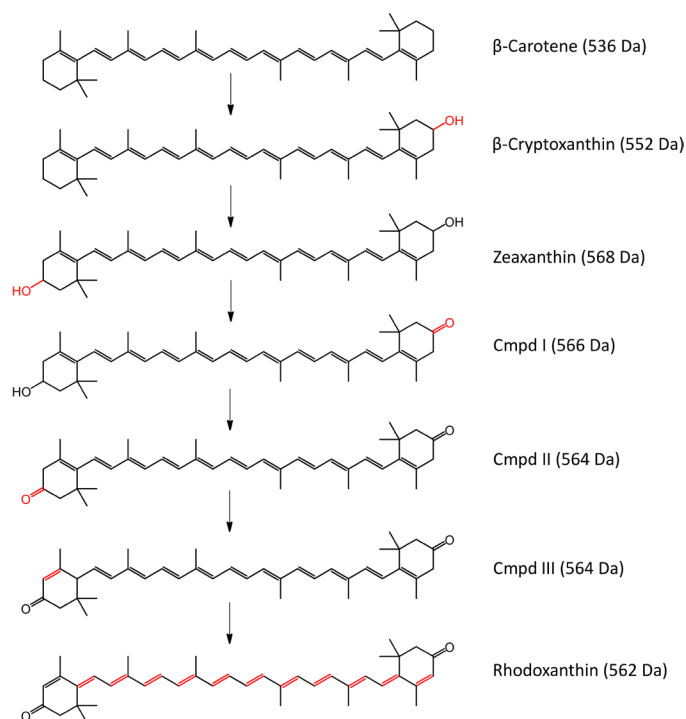


**Fig. 5. Proposed pathway from  $\beta$ -carotene to rhodoxanthin catalyzed by LHRS and mutant BCHs generated in this research.** Pathway is based on identification and progression of carotenoid accumulation described in Fig. 4 (A and B), fig. S6, and tables S3 and S4. Known compounds were identified based on comparisons to standards. Unknown Cmpds I, II, and III were tentatively identified based on chromatography, mass, spectra, and comparison to literature (20) as  $\beta$ ,  $\beta$ -carotene-3-ol, 3'-one,  $\beta$ ,  $\beta$ -carotene-3, 3'-dione, and  $\epsilon$ ,  $\beta$ -carotene-3, 3'-dione, respectively. Regions in red indicate specific modification at each step in the proposed pathway.

shift of 5 to 8 nm. The spectral shape of Cmpd III is similar to that of  $\alpha$ -carotene (1), consistent with the conversion of one ring from the  $\beta$  to the  $\epsilon$  configuration in the transition from Cmpd II to III. We have tentatively identified Cmpd III as  $\epsilon$ ,  $\beta$ -carotene-3,3'-dione (Fig. 5). The absorption maxima and spectral shapes of Cmpds II and III are identical or similar to those of chemically synthesized versions of these compounds (20), supporting our tentative identifications.

In the final conversion of Cmpd III or other mass 564 intermediate to rhodoxanthin, two additional hydrogens are lost with the introduction of an additional double bond and a concerted isomerization of the carotene backbone double bonds to the retro configuration (Fig. 5). None of the intermediates have the unique spectrum of rhodoxanthin, suggesting that the introduction of an additional double bond and the bond shift to the retro configuration occurs in the final step(s) in rhodoxanthin formation.

## DISCUSSION

While the presence of rhodoxanthin and other retro-carotenoids in plants (3–5, 8, 9) and birds (2, 6, 7, 21) is well documented, the basis for their synthesis has remained enigmatic. Here, we used a combined transcriptomics and proteomics approach to identify a honeysuckle BCH family enzyme (LHRS), the expression of which is linked to rhodoxanthin formation in red berries. We demonstrate that LHRS converts  $\beta$ -carotene to rhodoxanthin and propose

a biosynthetic pathway. Support for this comes from the following observations: (i) Transient expression of *LHRS* in *N. benthamiana* resulted in the accumulation of rhodoxanthin, (ii) expression of *LHRS* in  $\beta$ -carotene-accumulating *E. coli* resulted in the accumulation of rhodoxanthin, (iii) the substitution of three key residues implicated in rhodoxanthin formation within *LHRS* into the non-rhodoxanthin-forming *S. lycopersicum* BCH (CRTR-B2) conferred the ability to synthesize rhodoxanthin, and (iv) the recapitulation of these three residues determined to be key to rhodoxanthin formation in *LHRS* in a bacterial BCH (CrtZ) significantly boosted its innate rhodoxanthin-forming specificity.

The concurrence of rhodoxanthin accumulation and overexpression of a BCH-like enzyme rather than a P450-type hydroxylase suggested that  $\beta$ -carotene and zeaxanthin, rather than  $\alpha$ -carotene and lutein, are precursors for rhodoxanthin in honeysuckle. That the same enzyme that hydroxylated  $\beta$ -carotene to form zeaxanthin was also capable of performing the ketolation, desaturation, and double bond rearrangements necessary to convert  $\beta$ -carotene to rhodoxanthin was unexpected. The expression pattern and unusual sequence of *LHRS* contrasted with the typical *Lonicera* BCH, which was more highly expressed in leaves. *LHRS* is a unique, chromoplast-localized enzyme that appears to have diverged much earlier than typical chromoplastic BCHs and catalyzes a previously unknown enzymatic activity.

BCH enzymes are members of a functionally diverse class of diiron enzymes known to catalyze desaturations and hydroxylations (13, 22). In addition, this diverse group of enzymes shares transmembrane domains and diiron-coordinating histidine residues with more distantly related bacterial and algal enzymes involved in ketolation of  $\beta$ -carotene (10). The finding that a small number of amino acid substitutions cause large changes in catalytic activity is somewhat analogous to an earlier study where the substitution of four key residues converted a desaturase to a hydroxylase (23). However, the current case differs in that the substitution of three amino acids expands rather than converts activity, resulting in a multifunctional enzyme that retains the initial hydroxylase activity and acquires multiple new activities that lead to rhodoxanthin formation. A cytochrome P450 monooxygenase from *Xanthophyllomyces dendrorhous* that ketolates the ring C-4 carbon and hydroxylates the ring C-3 carbon to convert  $\beta$ -carotene to astaxanthin is an example of a multifunctional enzyme that is capable of both hydroxylation and ketolation (24). However, the combination of sequential hydroxylation, conversion of hydroxyl groups to keto groups, and desaturation and double bond rearrangements mediated by *LHRS* is, to our knowledge, without precedent. *LHRS* essentially mediates a complete multistep pathway from  $\beta$ -carotene to rhodoxanthin by a series of distinct oxidation steps, in which the product of each step becomes the substrate for the next catalytic cycle. Several successive oxidations have been reported for other multifunctional members of the membrane class of diiron enzymes. Examples include a *Hedera helix* (English ivy) desaturase that can perform  $\Delta 9$  followed by  $\Delta 4$  desaturation on stearoyl-ACP (acyl carrier protein) (25), a fungal membrane desaturase that sequentially inserts a  $\Delta 12$  followed by a  $\Delta 15$  double bond into oleoyl-PE (phosphatidylethanolamine) (26), and a multifunctional insect enzyme that functions as a  $\Delta 11$  desaturase,  $\Delta 11$  acetylenase, and  $\Delta 13$  desaturase (27).

Rhodoxanthin formation by the native bacterial CrtZ in our *E. coli* expression system was unexpected, because it was not reported in a previous published study (18). However, that it naturally contained one of the three residues identified in this study, and that al-

tering the remaining two critical residues dramatically increased rhodoxanthin accumulation, is consistent with their involvement in rhodoxanthin formation. Moreover, there is growing evidence that the catalytic activities of isolated carotenoid enzymes are highly dependent on biological context. In the previous study (18), CrtZ was introduced into *E. coli* as part of a gene cluster that also contained transglycosylases. These enzymes glycosylate  $\beta$ -cryptoxanthin and zeaxanthin, which would likely render them unsuitable as substrates for further oxidation to rhodoxanthin. A different *P. agglomerans* hydroxylase produced only the expected hydroxylation reactions in vitro, but synthesized additional compounds (presumed to be ketolated carotenoids) when expressed in *E. coli* (28).

Homology modeling of *LHRS* confirmed that it shares structural similarity with the crystallized fatty acid  $\alpha$ -hydroxylase (19). While amino acid identities between *LHRS* and the template are relatively low, the invariant histidine residues comprising the tripartite histidine motif characteristic of this class of integral membrane diiron enzymes superimpose between the fatty acid  $\alpha$ -hydroxylase and *LHRS* models, supporting its fidelity. The three key residues that control rhodoxanthin formation are located close to the putative substrate-binding cavity. Position 72 lines the cavity at its opening to solvent, while positions 102 and 103 are cavity-lining residues deep within the cavity. BCH has a nonpolar A at position 72, whereas *LHRS* has a polar residue, T. Hydrophobic residues are found at position 102, BCH having an aromatic F, in place of the aliphatic I found in *LHRS*, whereas residue 103 is occupied by an A in BCH, in place of the helix-breaking residue P, in *LHRS*. The model suggests that these critical residues are not catalytic but, instead, likely act by changing the binding orientation of the typical BCH product, zeaxanthin, as well as additional intermediates, to favor binding, ketolation, desaturation, and double bond rearrangement.

On the basis of order of accumulation, mass, and ultraviolet-visible spectra, we propose the intermediate structures and pathway to rhodoxanthin depicted in Fig. 5. The first steps, sequential hydroxylation of the rings of  $\beta$ -carotene to form  $\beta$ -cryptoxanthin and zeaxanthin, are the reactions of a typical BCH (29). The unique, extended oxidative pathway proposed for rhodoxanthin biosynthesis proceeds by sequential conversions of the hydroxyl groups of zeaxanthin to keto groups on alternating rings, followed by an isomerization to convert one ring from the  $\beta$  to the  $\epsilon$  form, and, ultimately, a desaturation leading to an additional double bond and concerted shift of bonds from the standard to the retro configuration to form rhodoxanthin. The geometry of the cavity of *LHRS* is consistent with oxidation reactions occurring only at a single end of the substrate. Thus, the transformation from  $\beta$ -carotene to rhodoxanthin would almost certainly require that the intermediates be released and rebound to allow oxidation of both of the rings. This binding-release-rebinding cycle likely accounts for the buildup of free intermediates in our time course experiments. Cmpd II ( $\beta$ ,  $\beta$ -carotene-3,3'-dione) was previously identified in rhodoxanthin-producing *Taxus arils* (8). Compounds with additional hydroxyl groups [loniceraxanthin, identified in *Lonicera* berries (9), and 6-hydroxy- $\epsilon$ , $\epsilon$ -carotene-3,3'-dione, identified in Pin-tailed Manakin feathers (21)], were not, however, observed in this work.

Hydrogen abstraction was previously posited as a mechanism for BCH-mediated hydroxylations of  $\beta$ -carotene to  $\beta$ -cryptoxanthin and zeaxanthin (29), and other members of the non-heme diiron-containing oxygenase class similarly use hydrogen abstraction for desaturations (30) and keto-enol isomerizations (31). Thus, the

same mechanism could plausibly catalyze multiple proposed steps in the oxidation of  $\beta$ -carotene to rhodoxanthin. Further, the multifunctionality demonstrated here for LHRS underscores the catalytic versatility of the integral membrane diiron family of enzymes.

It is intriguing that two enzymes related to BCHs that have unusual functions (LHRS and carotenoid beta ring 4-dehydrogenase, which is active in astaxanthin biosynthesis in *Adonis aestivalis*) are involved in the synthesis of red pigments (32). An association of red flowers with bird pollination (33) and a preference for red fruits by some birds (34) have been reported; thus, red fruits and flowers might confer a selective advantage to plants that are dependent on birds for seed and pollen dispersal. The appeal of rhodoxanthin-containing *Lonicera* berries to native North American bird species is evident from the novel, and perhaps fitness-altering, red feather pigmentation patterns recently emerging in species such as Cedar Waxwings (7) and Baltimore Orioles (6) that consume the red berries of these invasive honeysuckles. The appeal of this low-energy and elegantly symmetrical carotenoid molecule may extend further to human consumers in the near future, as rhodoxanthin is currently under development as a natural coloration substitute for artificial red dyes and beetle-derived carmine in candies, soft drinks, and cosmetics (35).

## MATERIALS AND METHODS

### Berry samples

Red and orange berries and green leaves were obtained from roadside *Lonicera* plants in Lexington, MA (Lex Red) and Bolton, MA (Bolton Red and Bolton Orange). Berries used for transcriptomic analysis were harvested and frozen immediately in liquid nitrogen in the field. Berries used for proteomic analysis were transported from the field to the laboratory on intact branches, placed at 4°C within 30 min of harvesting, and extracted within 24 hours. Berries used for carotenoid analysis were analyzed within several hours of harvesting, or stored at –80°C, while berries for ribosomal DNA (rDNA) analysis were lyophilized and stored at 4°C.

### Preparation and phylogenetic analysis of *Lonicera* rDNA

Lyophilized berries were first ground using a micropestle (Sigma-Aldrich, catalog no. 3 Z359947) in a 1.5-ml Eppendorf microcentrifuge tube. DNA extractions were performed using a modification of the Qiagen DNeasy Plant Mini Kit (Qiagen, Germany, catalog no. 69104). Samples were subjected to two centrifugations (2 min, 20,000g) through the QIAshredder Mini column. The Internal Transcribed Spacer 1 and 2 + 5.8S ribosomal RNA (rRNA) gene (ITS rDNA) was amplified using the primers ITS5 and ITS4 (36) using iProof High-Fidelity Master Mix (Bio-Rad, catalog no. 172-5310). Polymerase chain reaction (PCR) products were purified using Qiagen's PCR Gel Extraction Kit (catalog no. 28704) from a 2% agarose gel. PCR products were sequenced (Genewiz) using ITS 2, 3, 4, and 5 primers (36).

### Carotenoid analysis: Normal-phase HPLC methodology

Biological samples were extracted with tetrahydrofuran, evaporated to dryness, and resuspended in heptane:ethyl acetate:methylene chloride (2:2:1). A Waters 1525 binary pump attached to a Waters 717 plus or 2707 auto-sampler was used to inject samples. A Phenomenex Luna Silica (2) 3  $\mu$ m 150 mm  $\times$  4.6 mm column with a security silica guard column kit was used to resolve carotenoids with a Waters 2998 PDA detector. Synthetic carotenoid samples, purchased from CaroteNature (GmbH, Im Budler 8, CH-4419 Lupsingen,

Switzerland) or received from DSM Nutritional Products Ltd., were used as reference standards. The mobile phase consisted of 1000 ml of heptane, 60 ml of isopropanol, and 0.1 ml of acetic acid. The detector was a Waters 2998 photo-diode array detector from 210 to 600 nm.

### Mass spectrometry

We used a Thermo Fisher Scientific Q Exactive Focus MS using an atmospheric pressure chemical ionization source in positive ion mode. We collected at a resolution of 17,500 in positive ion mode, looking at the mass range between 250 and 1200 mass/charge ratio ( $m/z$ ). The HPLC method already described triggered the MS at inject start using a contact closure. The PDA detector out was connected directly to the MS via a divert valve.

### RNA isolation and sequencing

Flash-frozen berries were ground in liquid nitrogen using a mortar and pestle. Fifty to 100 mg of the resulting material were transferred to a 1.7-ml microcentrifuge tube. The RNAqueous Total RNA Isolation Kit (AM1912, Thermo Fisher Scientific), in combination with Ambion Plant RNA Isolation Aid (AM9690, Thermo Fisher Scientific), was used to extract total RNA from the berry samples following the manufacturers' protocols. The final elutions were further purified using the Qiagen RNeasy Plant Mini Kit (74904) following the manufacturer's protocol. The quality and quantity of the total RNA extracted were checked using the Agilent Bioanalyzer and RNA 600 Nano Kit with the instrument set to "fungal." Samples were sent to Tufts Genomic Center for mRNA sequencing analysis. The sequencing library construction was performed by Tufts using the TruSeq RNA Kit from Illumina. HiSeq Paired-End 150 and MiSeq Paired End 250 runs were performed.

### Sequence assembly, annotation, and expression data

De novo assembly of the Illumina sequence data including residual rRNA filtering, quality clipping, and  $\phi$ X174 filtering was performed with a development version of the MIRA assembler (37) based on version 4.9.5 (<https://sourceforge.net/projects/mira-assembler/files/MIRA/development/>). Annotation of resulting sequences  $\geq 300$  bases was performed by using a version of Prokka (38), modified to annotate transcript sequences, and with the entirety of UniProt/SwissProt and UniProt/TrEMBL (39) as underlying core database. Expression levels of genes were computed by mapping cleaned and trimmed Illumina sequence data normalized to 1.5 gigabases per sample against the annotated transcripts using MIRA and extracting median coverage numbers for annotated gene stretches from the result files.

### Proteomic analysis

Chromoplast-enriched fractions of berries used in proteomic studies were isolated according to a modification in (40). Fresh berries (125 g) were ground in a Waring blender (10 s, low speed) in 400 ml of ice-cold, modified GR buffer [50 mM Hepes, 330 mM sorbitol, 2 mM EDTA, 1 mM MgCl<sub>2</sub>, 1 mM MnCl<sub>2</sub>, and 2 mM dithiothreitol (pH 6.8)]. The homogenate was filtered through cheesecloth and Miracloth (Millipore) and centrifuged at 16,000g for 10 min. The pellet was resuspended in an equal volume of 30% Nycodenz (Axis-Shield PoC AS, Oslo, Norway), in GR buffer lacking sorbitol, and subjected to a discontinuous Nycodenz density gradient centrifugation (12.5, 10, 7.5, and 5%) at 7000g for 45 min in a swinging bucket rotor (Sorvall HB6). The 5% fraction containing most of the chromoplasts was

diluted in six volumes of GR buffer and clarified by centrifugation (7 min, 3000g). After decanting, pellets were resuspended in excess GR buffer and frozen at  $-80^{\circ}\text{C}$  before proteomic analysis. Proteomic analysis was outsourced to Biognosys (Zurich, Switzerland) following the procedure described in (41).

### Alignment and phylogenetic analysis of LHRS

Comparison BCH sequences were obtained from (32) supplemental dataset 1 or directly from the public database (39). Alignment of the amino acid sequences was done using MAFFT on XSEDE (7.305) through the CIPRES Science Gateway (42). Phylogenetic analysis of the BCH amino acid sequence data was done using maximum likelihood (ML), conducted in the program RAxML-HPC2 on XSEDE (8.2.10) through the CIPRES Science Gateway (42). The Protein Gamma model of rate heterogeneity applied to the dataset and branch support for the ML analyses was determined by 1000 bootstrap replicates.

### *N. benthamiana* transient expression system

*Lonicera* (Lex Red) red berry cDNA (350 pg) was used to amplify *BCHL* (LHRS; identified in transcriptome and deposited as GenBank MK982903) using primers MO11378 (CACACCCATGGCAACCGGAGTTCC) and MO11379 (CACACGGTGACCTTAATCCTCTTTTTTCACCTGCA). An 858-base pair fragment was amplified by PCR and cleaved using Nco I and Bst EII. The plant expression vector pCambia1304 (Marker Gene Technologies Inc.) was digested with Nco I and Bst EII and ligated to the BHyr Nco I–Bst EII fragment to produce pMB8085. *N. benthamiana* infiltration was done with LHRS plus P19 or with P19 alone as a control according to the protocol described in (43). Leaves were harvested 5 days after infiltration. Approximately 0.2 to 0.5 g of leaves were extracted in a 7-ml Precellys tube (Bertin Technologies) using 3 ml of heptane:ethyl acetate 1:1 plus 0.01% BHT (butylated hydroxytoluene). Extracts were analyzed by normal-phase HPLC.

### *E. coli* expression system

To enable lycopene synthesis, the insert of pAC-LYCi<sub>1</sub> (17) containing *crtE* (geranylgeranyl diphosphate synthase), *crtI* (phytoene dehydrogenase), *crtB* (phytoene synthase), and *idi* (isopentenyl-diphosphate delta-isomerase) of *P. agglomerans* (*Erwinia herbicola* Eho10) was synthesized with Not I ends and cloned into the Not I site of pET28a to create pMB8501 (GenScript). Expression of the above genes is under the control of the native promoters.

A truncated version lacking the presumed chloroplast-targeting sequence (residues 2 to 30) of the  $\beta$ -carotene cyclase gene *LCY-B* (identified in the *Lonicera* transcriptome and proteome and deposited as GenBank MK2982904) was amplified from Lex Red red berry cDNA with primers MO11207 (CACACCATATGCCCA-CAAAAAGGTCTCTC) and MO11206 (CACACCCTAGGT-CAAATGGATTCAAGTGCAA), which generated an Nde I site at the 5' end and an Avr II site on the 3' end. The resulting PCR product was digested with Nde I and Avr II and cloned into the identical sites of pCDFDuet-1 (Novagen) to generate plasmid pMB8103. Expression of the cyclase gene is under the control of the T7 promoter.

Truncated LHRS lacking the presumed chloroplast-targeting sequence (amino acids 2 to 81) was amplified from Lex Red red berry cDNA using primers MO11211 (CACACCCATGGAGAGAACA-GAGAGAAAGAGAA) and MO11212 (CACACCTTAAGTTA-ATCCTCTTTTTTCACCTGC). The PCR product was digested with

Nco I and Afl III and subcloned into pACYCDuet-1 (Novagen) digested with the same enzymes, resulting in pMB8088.

Truncated *S. lycopersicum* CRTR-B2 (GenBank Y14810) lacking the presumed chloroplast-targeting sequence (amino acids 2 to 97) and full-length, *E. coli*-optimized *CrtZ* (UniProtKB Q01332) were synthesized and subcloned into the Nco I and Avr II sites of pACYCDuet-1 by GenScript. Specific mutageneses of the above genes were performed on the synthesized unmutated sequences by GenScript.

Competent BL21 (DE3) cells were purchased from New England Biolabs. Additional strains were made competent and transformed using standard methods (44). Antibiotic concentrations in liquid and plate culture were as follows: kanamycin (25  $\mu\text{g}/\text{ml}$ ), spectinomycin (25  $\mu\text{g}/\text{ml}$ ), and chloramphenicol (17  $\mu\text{g}/\text{ml}$ ). For carotenoid production, strains were grown in Overnight Express Autoinduction medium (Novagen) in LB with antibiotic in un baffled flasks (20 ml of medium, 125 ml flasks) at  $25^{\circ}\text{C}$  (250 rpm) for 34 to 40 hours unless indicated. Samples (15 ml) were centrifuged (4000 rpm, 5 min), and pellets were extracted immediately (for MS) or stored at  $-80^{\circ}\text{C}$ . For extraction, pellets were vortexed with 3 ml of HPLC mobile phase (see above) and transferred to 7 ml Precellys (Bertin Technologies) extraction tubes. After incubation at  $-80^{\circ}\text{C}$  for at least 15 min, samples were extracted on a Precellys homogenizer at 7500 rpm,  $3 \times 15$ -s bursts with 5-s pauses. Samples were next centrifuged, and the supernatants were transferred to glass vials and evaporated to dryness. Dried samples were dissolved in 40  $\mu\text{l}$  of methylene chloride and 140  $\mu\text{l}$  of HPLC mobile phase and analyzed by normal-phase HPLC.

### Structural modeling of LHRS

A homology model was constructed in the molecular modeling program Yasara (YASARA Biosciences GmbH, Vienna, Austria, 2018) using a manually curated alignment of the LHRS sequence and the template crystal structure of the integral membrane fatty acid  $\alpha$ -hydroxylase [18.8% identity, 34.7% similarity, Protein Data Bank code 4ZR1 (19)]. Despite low sequence identity, the catalytic His-metal cluster and the four transmembrane helices are conserved between both enzymes. Figure 3D was prepared using the Schrodinger molecular modeling suite (Maestro 11.5, Schrodinger LLC, New York, NY 2018).

### Accession numbers

Sequence data from this article can be found in the GenBank/UniProt data libraries under the following accession numbers. cDNA: *S. lycopersicum* chromoplast *BCH* CRTR-B2, Y14810, *Lonicera* LYC-B, \*MK982904, *Lonicera* BCH, \*MK982903, *Lonicera* LHRS, \*MK982903. Genomic DNA: *P. agglomerans* *crtE*, *crtI*, *crtB*, *idi*, GenBank M87280.1. Polypeptides: *S. lycopersicum* chromoplast *BCH*, (SL-2) CRTR-B2, CAB55626; *Zea mays* ZMCRTRB3, AFD18929; *Arabidopsis thaliana* BCH2, NP\_200070; *Vitis vinifera* BCH1, NP\_001268126; *S. lycopersicum* CRTR-B1, NP\_001234348; *P. agglomerans* *crtZ*, UniProtKB Q01332. *Lonicera* ITS sequences: Bolton Red, \*MK967966; Bolton Orange, \*MK967967; Lex Red, \*MK967965. \* indicates sequences deposited in this work.

### SUPPLEMENTARY MATERIALS

Supplementary material for this article is available at <http://advances.sciencemag.org/cgi/content/full/6/17/eaay9226/DC1>

[View/request a protocol for this paper from Bio-protocol.](#)

## REFERENCES AND NOTES

- G. Britton, S. Liaaen-Jensen, H. E. Pfander, *Carotenoids Handbook* (Birkhäuser Basel, 2004), 647 pp.
- C. J. Berg, A. M. LaFountain, R. O. Prum, H. A. Frank, M. J. Tauber, Vibrational and electronic spectroscopy of the retro-carotenoid rhodoxanthin in avian plumage, solid-state films, and solution. *Arch. Biochem. Biophys.* **539**, 142–155 (2013).
- H. H. Strain, Eschscholtzanthin: A new xanthophyll from the petals of the California poppy, *Eschscholtzia californica*. *J. Biol. Chem.* **123**, 425–437 (1938).
- B. Czeuczuga, Different rhodoxanthin contents in the leaves of gymnosperms grown under various light intensities. *Biochem. Syst. Ecol.* **15**, 531–533 (1987).
- M. Diaz, E. Ball, U. Luttge, Stress-induced accumulation of the xanthophyll rhodoxanthin in leaves of *Aloe vera*. *Plant Physiol. Biochem.* **28**, 679–682 (1990).
- J. Hudon, D. Derbyshire, S. Leckie, T. Flinn, Diet-induced plumage erythrisms in Baltimore orioles as a result of the spread of introduced shrubs. *Wilson J. Ornithol.* **125**, 88–96 (2013).
- A. H. Brush, A possible source for the rhodoxanthin in some cedar waxwing tails. *J. Field Ornith.* **61**, 355 (1990).
- R. Kuhn, H. Brockmann, Ueber Rhodo-xanthin, den Arillus-Farbstoff der Eibe (*Taxus baccata*). *Eur. J. Inorg. Chem.* **66**, 828–841 (1933).
- A.-K. Rahman, K. Egger, Ketocarotinoide in den Früchten von *Lonicera webbiana* und *Lonicera ruprechtiana*. *Z. Naturforsch.* **28**, 434–436 (1973).
- F. X. Cunningham Jr., E. Gant, Genes and enzymes of carotenoid biosynthesis in plants. *Annu. Rev. Plant. Physiol. Plant Mol. Biol.* **49**, 557–583 (1998).
- J. Hirschberg, Carotenoid biosynthesis in flowering plants. *Curr. Opin. Plant Biol.* **4**, 210–218 (2001).
- A. R. Moise, S. Al-Babili, E. T. Wurtzel, Mechanistic aspects of carotenoid biosynthesis. *Chem. Rev.* **114**, 164–193 (2014).
- F. Bouvier, Y. Keller, B. d'Harlingue, B. Camara, Xanthophyll biosynthesis: Molecular and functional characterization of carotenoid hydroxylases from pepper fruit (*Capsicum annuum* L.). *Biochim. Biophys. Acta* **1391**, 320–328 (1998).
- N. Galpaz, G. Ronen, Z. Khalfa, D. Zamir, J. Hirschberg, A chromoplast-specific carotenoid biosynthesis pathway is revealed by cloning of the tomato *white-flower* locus. *Plant Cell* **18**, 1947–1960 (2006).
- H. Hudon, A. Storni, E. Pini, M. Anciaes, R. Stradi, Rhodoxanthin as a characteristic keto-carotenoid of manakins (Pipridae). *The Auk* **129**, 491–499 (2012).
- J. Shanklin, E. Whittle, B. Fox, Eight histidine residues are catalytically essential in a membrane-associated iron enzyme, stearyl-coA destaurase, and are conserved in alkane hydroxylase and xylene monooxygenase. *Biochemistry* **33**, 12787–12794 (1994).
- F. X. Cunningham Jr., H. Lee, E. Gant, Carotenoid biosynthesis in the primitive red alga *Cyanidioschyzon merolae*. *Eukaryot. Cell* **6**, 533–545 (2007).
- B. S. Hundle, P. Beyer, H. Kleinig, G. Englert, J. E. Hearst, Carotenoids of *Erwinia herbicola* and an *Escherichia coli* HB101 strain carrying the *Erwinia herbicola* carotenoid gene cluster. *Photochem. Photobiol.* **54**, 89–93 (1991).
- G. Zhu, M. Koszelak-Rosenblum, S. M. Connelly, M. E. Dumont, M. G. Malkowski, The crystal structure of an integral membrane fatty acid  $\alpha$ -hydroxylase. *J. Biol. Chem.* **290**, 29820–29833 (2015).
- J. D. Surmatis, A. Walsler, J. Gibas, U. Schweiter, R. Thommen, New methods for the synthesis of oxygenated carotenoids. *Helv. Chim. Acta* **53**, 974–990 (1970).
- J. Hudon, M. Anciães, V. Bertacche, R. Stradi, Plumage carotenoids of the Pin-tailed Manakin (*Ilicura militaris*): Evidence for the endogenous production of rhodoxanthin from a colour variant. *Comp. Biochem. Physiol. B Biochem. Mol. Biol.* **147**, 402–411 (2007).
- J. Shanklin, E. B. Cahoon, Desaturation and related modifications of fatty acids<sup>1</sup>. *Annu. Rev. Plant. Physiol. Plant Mol. Biol.* **49**, 611–641 (1998).
- J. A. Broadwater, E. Whittle, J. Shanklin, Desaturation and hydroxylation. Residues 148 and 324 of *Arabidopsis* FAD2, in addition to substrate chain length, exert a major influence in partitioning of catalytic specificity. *J. Biol. Chem.* **277**, 15613–15620 (2002).
- K. Ojima, J. Breitenbach, H. Visser, Y. Setoguchi, K. Tabata, T. Hoshino, J. van den Berg, G. Sandmann, Cloning of the astaxanthin synthase gene from *Xanthophyllomyces dendrorhous* (*Phaffia rhodozyma*) and its assignment as a  $\beta$ -carotene 3-hydroxylase/4-ketolase. *Mol. Genet. Genomics* **275**, 148–158 (2006).
- J. E. Guy, E. Whittle, D. Kumaran, Y. Lindqvist, J. Shanklin, The crystal structure of the ivy  $\Delta^4$ -16:0-ACP desaturase reveals structural details of the oxidized active site and potential determinants of regioselectivity. *J. Biol. Chem.* **282**, 19863–19871 (2007).
- Y. Cai, X.-H. Yu, Q. Liu, C.-J. Liu, J. Shanklin, Two clusters of residues contribute to the activity and substrate specificity of Fm1, a bifunctional oleate and linoleate desaturase of fungal origin. *J. Biol. Chem.* **293**, 19844–19853 (2018).
- M. Serra, B. Piña, J. L. Abad, F. Camps, G. Fabriás, A multifunctional desaturase involved in the biosynthesis of the processionary moth sex pheromone. *Proc. Natl. Acad. Sci. U.S.A.* **104**, 16444–16449 (2007).
- G. H. Song, S. H. Kim, B. H. Choi, S. J. Han, P. C. Lee, heterologous carotenoid-biosynthetic enzymes: Functional complementation and effects on carotenoid profiles in *Escherichia coli*. *Appl. Environ. Microbiol.* **79**, 610–618 (2013).
- L. Tian, D. DellaPenna, Progress in understanding the origin and functions of carotenoid hydroxylases in plants. *Arch. Biochem. Biophys.* **430**, 22–29 (2004).
- J. Shanklin, J. E. Guy, G. Mishra, Y. Lindqvist, Desaturases: Emerging models for understanding functional diversification of diiron-containing enzymes. *J. Biol. Chem.* **284**, 18559–18563 (2009).
- F. G. Cantú Reinhard, P. Barman, G. Mukherjee, J. Kumar, D. Kumar, C. V. Sastri, S. P. de Visser, Keto-enol tautomerization triggers an electrophilic aldehyde deformation reaction by a nonheme manganese(III)-peroxo complex. *J. Am. Chem. Soc.* **139**, 18328–18338 (2017).
- F. X. Cunningham Jr., E. Gant, Elucidation of the pathway to astaxanthin in the flowers of *Adonis aestivalis*. *Plant Cell* **23**, 3055–3069 (2011).
- H. Sheehan, K. Hermann, C. Kuhlmeier, Color and scent: How single genes influence pollinator attraction. *Cold Spring Harb. Symp. Quant. Biol.* **77**, 117–133 (2012).
- Q. Duan, E. Goodale, R.-C. Quan, Bird fruit preferences match the frequency of fruit colours in tropical Asia. *Sci. Rep.* **4**, 5627 (2014).
- H. Grass, A. Hitzfeld, Red colorant for beverages, food and pharmaceutical compositions. Patent WO2015044213A1 (2015).
- T. J. White, T. Bruns, S. Lee, J. Taylor, Amplification and direct sequencing of fungal ribosomal RNA genes for phylogenetics, in *PCR Protocols: A Guide to Methods and Applications*, M. A. Innis, D. H. Gelfand, J. J. Sninsky, T. J. White, Eds. (Academic Press, 1990), pp. 315–332.
- B. Chevreux, T. Pfisterer, B. Drescher, A. J. Driesel, W. E. H. Müller, T. Wetter, S. Suhai, Using the miraEST assembler for reliable and automated mRNA transcript assembly and SNP detection in sequenced ESTs. *Genome Res.* **14**, 1147–1159 (2004).
- T. Seemann, Prokka: Rapid prokaryotic genome annotation. *Bioinformatics* **30**, 2068–2069 (2014).
- The UniProt Consortium, UniProt: The universal protein knowledgebase. *Nucleic Acids Res.* **45**, D158–D169 (2017).
- Y. Zeng, Z. Pan, Y. Ding, A. Zhu, H. Cao, Q. Xu, X. Deng, A proteomic analysis of the chromoplasts isolated from sweet orange fruits [*Citrus sinensis* (L.) Osbeck]. *J. Exp. Bot.* **62**, 5297–5309 (2011).
- R. Bruderer, O. M. Bernhardt, T. Gandhi, Y. Xuan, J. Sondermann, M. Schmidt, D. Gomez-Varela, L. Reiter, Optimization of experimental parameters in data-independent mass spectrometry significantly increases depth and reproducibility of results. *Mol. Cell. Proteomics* **16**, 2296–2309 (2017).
- M. A. Miller, W. Pfeiffer, T. Schwartz, Creating the CIPRES Science Gateway for inference of large phylogenetic trees, in *Proceedings of the Gateway Computing Environments Workshop (GCE)* (IEEE, 2010), pp. 1–8.
- K. Schütze, K. Harter, C. Chaban, Bimolecular fluorescence complementation (BiFC) to study protein-protein interactions in living plant cells, in *Methods in Molecular Biology*, T. Pfannschmidt, Ed. (Humana Press, 2009), vol. 479, pp. 189–202.
- J. Sambrook, T. Fritsch, T. Maniatis, *Molecular Cloning: A Laboratory Manual* (Cold Spring Harbor, 1989).

**Acknowledgments:** We acknowledge the contribution of J. Schierle regarding carotenoid structure, analysis and characterization, useful discussions on protein structure with W.E. Royer, as well as inspiration and encouragement from M. Tavares. **Funding:** DSM funded this research. **Author contributions:** J.R. and B.C. conceived the study. J.R., M.M., P.H., B.C., L.L., J.M., P.B., N.B.-K., T.B., R.M.d.J., K.L., Y.C., and J.T. performed experiments. J.R. and J.S. interpreted data and wrote the manuscript. **Competing interests:** The authors declare that they have no competing interests. WO2019016384, NOVEL ENZYME, contains a portion of the results presented in this paper. J.S. had a consulting agreement with DSM. **Data and materials availability:** All data needed to evaluate the conclusions in the paper are present in the paper and/or the Supplementary Materials. Additional data related to this paper may be requested from the authors.

Submitted 29 July 2019

Accepted 31 January 2020

Published 22 April 2020

10.1126/sciadv.aay9226

**Citation:** J. Royer, J. Shanklin, N. Balch-Kenney, M. Mayorga, P. Houston, R. M. de Jong, J. McMahon, L. Laprade, P. Blomquist, T. Berry, Y. Cai, K. LoBuglio, J. Trueheart, B. Chevreux, Rhodoxanthin synthase from honeysuckle; a membrane diiron enzyme catalyzes the multistep conversion of  $\beta$ -carotene to rhodoxanthin. *Sci. Adv.* **6**, eaay9226 (2020).